I.J. Wireless and Microwave Technologies, 2026, 5, 284-298
Published Online on October 8, 2026 by MECS Press (http://www.mecs-press.org/)
DOI: 10.5815/ijwmt.2026.05.17

Thermal-Corrected Hyperspectral Analysis of Lunar Surface Hydration and Mineralogy Using Chandrayaan-2 IIRS and Chandrayaan-1 M^3 Data

Saritha Mulkala
Department of Electronics and Communication Engineering, National Institute of Technology Warangal, Warangal, 506004, Telangana, India
E-mail: ms23ecr1r13@student.nitw.ac.in
ORCID iD: https://orcid.org/0000-0002-5569-0331

Anjaneyulu Lokam
Department of Electronics and Communication Engineering, National Institute of Technology Warangal, Warangal, 506004, Telangana, India
E-mail: anjan@nitw.ac.in
ORCID iD: https://orcid.org/0000-0001-7709-4365

Kiran Dasari*
Manipal Institute of Technology, Manipal Academy of Higher Education, Manipal, India
E-mail: kiran.dasari@manipal.edu
ORCID iD: https://orcid.org/0000-0002-3680-8058
*Corresponding Author

Prasanna Chandrika Chenuboyina
Department of Electronics and Communication Engineering, National Institute of Technology Warangal, Warangal, 506004, Telangana, India
E-mail: cp25ecm3s03@student.nitw.ac.in
ORCID iD: https://orcid.org/0009-0006-7410-3493

Received: May 7, 2026; Revised: June 18, 2026; Accepted: August 27, 2026; Published: October 8, 2026

Abstract: Information about the mineral makeup and whether the surface has water-related compounds can be obtained from the lunar surface's spectral reflectance. The Chandrayaan-2 Imaging Infrared Spectrometer (IIRS) and Chandrayaan 1 Moon Mineralogy Mapper (M^3) are hyperspectral instruments that can capture detailed spectral signatures across a wide range of wavelengths, from visible to infrared. This lets scientists' study lunar materials in great detail. This paper presents a systematic methodology for analyzing and interpreting the hyperspectral data from Indian lunar missions to derive significant reflectance data. The workflow includes converting measured radiance to reflectance, applying photometric adjustments, removing thermal radiation contributions using the Planck-based model, and getting spectra from certain pixels in selected lunar areas. To study two sites, IIRS images were taken from the following two craters: Gardner crater and Glauber crater. Glauber Crater's images facilitated a direct comparison between the two missions. From the spectrum produced, the presence of iron-based lunar rocks like olivine and pyroxene can be identified. The absorption dip observed in Gardner crater within the 3 μm band proves the presence of hydroxyl or water on the surface. On the other hand, Glauber Crater lacks an absorption dip, indicating it is dry. The spectra obtained from IIRS and data are similar in spectral shape over the same area, indicating that both instruments independently confirm the absence of hydration for characterizing the lunar surface composition. With these findings, we gain insight into the Moon's mineral content and composition, variations in mineral properties from one area to another, and the presence of water signatures that depend on topography. The thermally corrected IIRS spectrum of Gardner crater reveals a characteristic absorption feature at 3 μm centred at 2.918 μm with band depth of 0.072 and FWHM of 0.194 μm, suggesting that there is surface OH/O on Gardner crater as has been detected before by IIRS hydration features at similar latitudes of the Moon. On the other hand, the spectra from both IIRS and M^3 at Glauber crater reveal only an increase in the slope of the spectrum without showing any 3 μm hydration absorption feature. The IIRS reflectance ranges from 0.025 to 0.200 while the M^3 reflectance ranges from 0.015 to 0.038. This is expected due to variations in calibration of the two sensors; however, in this case it shows consistency in the fact that there is no surface hydration.

This work is open access and licensed under the Creative Commons CC BY 4.0 License.

Index Terms: Lunar, Chandrayaan-1, Chandrayaan-2, Imaging Infrared Spectrometer, Moon Mineralogy Mapper, Gardner crater, Glauber crater

1. Introduction

The Moon serves as a preserved archive of the formation period of our Solar System, and it has remained largely unaffected by tectonic movements or weathering, which is why it serves as an excellent target for planetary geology [1]. Remote sensing of Earth's surface composition in the visible to near-infrared region (0.4 to 5 μm) is the most efficient technique because rock-forming silicates absorb energy in this band. The absorption lines for pyroxenes, abundant in mare basalts, are observed at 1 μm and 2 μm. Other important rocks, such as olivine and plagioclase feldspars that dominate the highland crust, have distinctive absorption lines that have been well documented by Apollo missions' spectroscopic analysis [2].

The Indian space mission Chandrayaan-1 (launched October 2008) has made great strides in this area by deploying the Moon Mineralogy Mapper (M^3), which acquired hyperspectral images of the entire Moon at wavelengths from 405 to 3000 nm, revealing, for the first time, the presence of absorption bands associated with OH/H2O near 3 μm [2,3,4]. But the spectral range for ended right in the middle of the hydration band, meaning that thermal emission characterization was not possible, and it was not possible to differentiate between surface hydroxyl and water/ice.[5]. These constraints directly led to the development of the Imaging Infrared Spectrometer (IIRS) in the Indian Chandrayaan-2 mission, launched in July 2019. IIRS works over 256 continuous spectral channels ranging from 0.8 to 5.0 μm at 80 meters spatial resolution and 20 kilometers swath width from a 100-kilometer polar orbit [1]. Its long-wavelength spectral range allows it to simultaneously estimate surface temperatures using thermal bands between 4.5 and 4.9 μm, thus allowing internal physical thermal correction, which was impossible with [6].

However, deriving surface reflectance from Level 1 radiance data of IIRS remains a challenge. Thermal radiation becomes dominant beyond 2.5 μm, and for common day-side temperatures ranging between 250 and 400 K, the effects of thermal radiation become significant enough to overshadow actual hydration absorption bands [6]. In addition, photometric correction of observation geometries and calibration to the Apollo landing site reference spectra are also needed for cross-mission and cross-terrain comparisons [5]. Although previous research has investigated individual preprocessing steps, a validated and integrated preprocessing pipeline for various lunar terrains using $\mathbf{M^3}$ is still an ongoing demand [2,5,6].

This paper seeks to fill this gap by conducting a detailed analysis of the spectral reflectance of Gardner crater (near side) and Glauber crater (far-side) using the IIRS Level-1 product with M^3 data at Glauber crater cross-validated. The entire workflow involves radiance to reflectance transformation, Planck thermal correction, photometric correction, and spectral extraction on a per pixel basis. The specific objectives include: testing the IIRS full processing chain workflow; identifying the mineral absorption bands for both craters; detecting and interpreting the 3 μm band; and demonstrating the spectral coherence of olivine/plagioclase in IIRS and [7]. The main result of this work, the detection of the 3 μm band hydration absorption for Gardner but not for Glauber, provides direct proof of spatial variability in the hydration status of the lunar surface, thus illustrating the potential of the IIRS instruments in the context of lunar exploration**.**

Some of the recent developments in IIRS data processing have further enhanced the capabilities of Chandrayaan-2 in characterizing the lunar surface. A photometric correction approach specific to IIRS data was developed by Bose et al. (2024) [8], and they found that IIRS reflectance values after correction exhibit less variability than those in M^3 Level-2 datasets. An automated selenoreferencing approach using the Python language for Chandrayaan-2 hyperspectral data cubes was presented by Rajgor et al., (2024) [9], thereby increasing the reproducibility of the IIRS-based processing chain. In another study, Rajasekhar et al., (2024) [10] carried out a thorough analysis of the Chandrayaan-3 landing site using IIRS data, showing the spatial variability in the hydration signatures on the morphologically different terrain units. Unlike all the above-mentioned works, the current study utilizes an end-to-end processing pipeline using IIRS Level-1 data on two geologically different craters with cross-validation using the M^3 Level-2 data and emissivity sensitivity analysis which are not considered in earlier preprocessing chains like that of Verma et al., (2022) [11].

Although Verma et al. (2022) [11] provided the basis for thermal correction through inversion technique based on Planck law and showed 3 μm hydration detection at various latitudes, this study takes the above-mentioned concept further and uses it on two different geological craters having varied hydration environments, performs cross validation with M^3 Level-2 data, and conducts an emissivity sensitivity study demonstrating that the band depth remains constant within the emissivity range of 0.85-0.99 for the Moon.

The particular contributions of this work are as follows: (i) an end-to-end processing framework for IIRS Level-1 radiance-to-reflectance transformation including Planck thermal correction [9]; (ii) empirical identification and estimation of the 3 μm hydroxyl absorption band in Gardner crater with BD = 0.072, absorption band position at 2.918 μm, and FWHM of 0.194 μm; (iii) evidence of spatial heterogeneity of lunar surface hydration using a comparison between hydrated (Gardner crater) and dry (Glauber crater) craters located on the near side and far side of the Moon [10]; (iv) validation of spectral trends obtained from the IIRS data against Chandrayaan-1 M^3 Level-2 reflectance measurements

[8]; and (v) sensitivity analysis proving that the estimated band depth does not depend on the choice of emissivity in the interval of 0.85–0.99.

2. Data Used

Two hyperspectral data sets from the Chandrayaan series of missions to the Moon from India, complementing each other, are used as the basis for observations in this work. The first data set is provided in the form of a calibrated radiance data set Level-1 obtained with the Imaging Infrared Spectrometer (IIRS) on board the Chandrayaan-2 (Ch-2) orbiter. The second data set is the reflectance data set Level-2 measured by Moon Mineralogy Mapper (M^3) onboard Chandrayaan-1 (Ch-1).

Table 1. Chandrayaan-2 IIRS Dataset Specifications

Parameter	Gardner Crater	Glauber Crater
Product ID	ch2_iir_nci__20250803T1115281307_d_img_d18	ch2_ iir_ nci _20191202T0639493114 _d _img _d18
Bands	256	256
Solar Incidence	33.81^0	36.71^0
Geographic Extent	17.7^0N– 33.8^0E	11.5^0 N– 142.6^0E,

Table 2. M^3 Dataset Specifications

Parameter	Value
Product ID	M3G20090528T213152V01
Bands	85
Product Level	Reflectance (Level-2)

IIRS is an array of dispersive hyperspectral sensors based on gratings that gather data along a 100 km circular polar orbit, with a ground sampling distance of around 80 m and swath width of 20 km [1]. It covers a spectral range of 0.8 to 5.0 μm in roughly 256 contiguous bands at a spectral resolution of 20 to 25 nm, making it the most spectrally extended orbital imaging spectrometer for mapping the Moon at this spatial detail [6]. The focal plane uses a detector array of mercury cadmium telluride (HgCdTe) actively cooled to 90 K, and a four-band order-sorting filter (OSF) is incorporated near the detector to suppress stray higher-order grating contributions and reduce instrument background [1]. Level-0 (raw telemetry), Level-1 (radiometrically calibrated, dark-corrected, and geometrically tagged radiance in $\mathbf{mWcm^{-2}\,\mu m^{-1}sr^{-1}}$), Level-2(thermally and photometrically corrected reflectance) [6]. The present work uses Level-1 data acquired in the E1G2 (exposure-1, gain-2) mode, which provides a wider dynamic range suitable for observations of equatorial-to-mid-latitude. Two IIRS scenes were selected: one covering Gardner crater and another Glauber crater.

The M^3 instrument, a NASA guest payload onboard Ch-1, operates in the spectral range of 405 to 3000 nm at a spatial resolution of approximately 140 m per pixel in global mode (85 bands) [12,13]. Its Level-2 reflectance product is photometrically calibrated and provides a well-validated benchmark against which new sensors are routinely assessed [14].

Two impact craters with contrasting geological settings were chosen to investigate the spatial variability of lunar mineralogy and surface hydration.

2.1. Gardner Crater

Gardner is an impact crater of Eratosthenian age (25 km diameter) situated at 17.7°N, 33.8°E on the near side of the Moon, positioned to the east of the Vitruvius crater and south-east of the landing site of Apollo 17 in the Taurus Littrow valley [15]. The crater exhibits a well-preserved morphology with steep inner walls, a flat floor, and elevated rim structures. Spectroscopic analysis using Ch-1 M^3 data had previously identified Gardner as the largest known central vent volcanic site on the lunar surface, with the underlying feeder dykes of the eastern Procellarum KREEP Terrain (PKT) thought to be its probable magmatic source [15]. The western inner flank of the crater is dominated by gabbroic material with high calcium pyroxene (HCP) with dual absorption features near 970 to 989 nm and 2137 nm, while low-calcium pyroxene (LCP) outcrops with absorptions near 930 to 940 nm and 2018 nm are locally exposed along its southern rim [15]. The mature highland regolith is prominent along the north-western rim. The spectral diversity of Gardner, combined with the availability of high-quality IIRS coverage, makes it particularly well suited to investigating hydration signatures alongside mafic mineral characterization.

2.2. Glauber Crater

Glauber is a relatively small circular impact crater (15 km in diameter) located on the far side of the Moon at 11.5°N, 142.6°E, within the outer rim of the Mendeleev Plain at equatorial latitudes [2,16]. Its floor spans approximately 5 km

and is dominated by the flat geological unit of the Nectarian Basin Massif, composed of lunar regolith, while the crater itself belongs to the Eratosthenian crater unit, characterized by debris and rocky material in its interior [14]. The walls of Glauber exhibit an immature (younger) regolith on steep slopes, whereas the flat exterior and crater floor are occupied by a mature, spectrally featureless regolith. Earlier IIRS and M^3 analyses have identified clinopyroxene along the crater wall and pigeonite-type LCP within a small interior crater, with abundance maps from spectral unmixing showing strong agreement between the two sensors [14]. Importantly, co-registration of IIRS and M^3 images over a common region near the southeast of the Taurus-Littrow valley allows direct pixel-level comparison, making Glauber an ideal validation site [14].

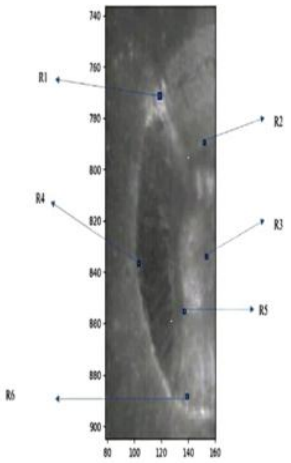


Fig. 1. Gardner Crater - IIRS

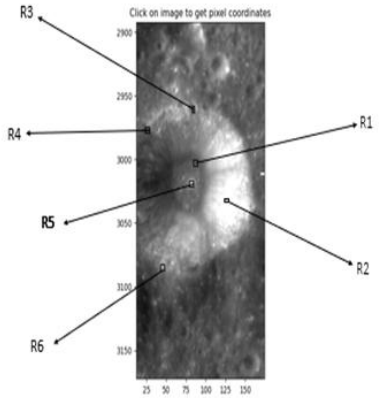


Fig. 2. Glauber Crater- IIRS

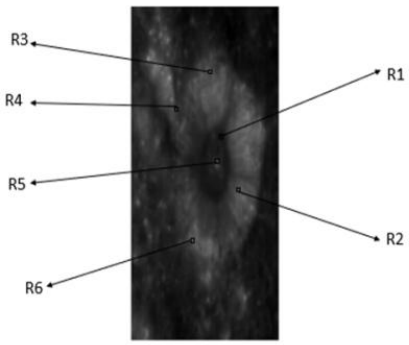


Fig. 3. Glauber Crater - M^3

Fig. 1., Fig. 2., and Fig. 3., show the Gardner and Glauber craters with selected pixel locations (R1-R6) used for spectral analysis across different regions of the surface. Fig. 1 presents Gardner crater from IIRS. Fig. 2 presents the Glauber crater from IIRS. Fig. 3 presents Glauber crater from M3 data, enabling comparison with IIRS observations for validation of spectral results.

3. Methodology

A multi-stage spectral processing pipeline was implemented in Python to transform raw IIRS Level-1 radiance cubes into reflectance spectra that could be interpreted scientifically. The same procedure was applied consistently at both test sites, and its results were later compared against the M^3 Level-2 reflectance spectra of Glauber crater.

3.1. Radiance-to-Reflectance Conversion

The measured spectral radiance L(λ) observed by IIRS at each pixel was transformed into the apparent spectral reflectance R(λ) using the conventional photometric equation used in all lunar hyperspectral observations [6,14]:

$$R(\lambda) = \frac{\pi D^2 L(\lambda)}{F_o(\lambda)cos(\theta)} \quad (1)$$

Here, $F_0(\lambda)$ is the spectral irradiance of the Sun at 1 AU and is taken from the high-resolution solar reference spectrum by Kurucz (1995) as implemented in the IIRS Level-1 header file and in agreement with the solar flux reference used for M³ data processing [13]. The quantity D stands for the distance between the Sun and Moon in Astronomical Units and can be found from the geometry of the scene available in the IIRS image strip header files. θ stands for the solar incidence angle. The constant factor of π converts the bidirectional reflectance factor into a hemispherical albedo under the Lambertian assumption [17,18]. This procedure is essentially identical to that applied to M^3data analysis [14] and has been confirmed for IIRS by [5,2].

The spectral solar irradiance $F_0(\lambda)$ employed in Eq. (1) is the solar extraterrestrial spectrum standardized in the Chandrayaan-2 IIRS radiometric calibration scheme as stated by Chowdhury et al. (2020) [1]. Level-1 IIRS radiance data products are derived from the ISRO radiometric calibration workflow that involves detector and geometric calibrations before dissemination. In this study, the radiance values at the Level-1 stage were converted to reflectance using Eq. (1). The derived reflectance spectra were scaled using the standardized IIRS scaling factor of 10^{-4} [1].

3.2. Thermal Emission Modeling and Correction

Beyond the wavelength range of about 2.5 μm, the thermal radiation emitted from the illuminated side of the Moon's surface cannot be neglected and acts as a disturbing factor to the mineral absorption lines [6,11]. The total measured radiance $L_{measured}(\lambda)$ was decomposed into its reflected ($L_{reflected}$) and thermally emitted ($L_{thermal}$) components. A key advantage of IIRS over earlier instruments such as M^3 is its 4.5 to 5.0 μm window, where the reflected solar irradiance is negligible under all realistic lunar surface conditions, so the sensor records essentially pure thermal emission in that range [11]. Thermal emission follows Planck's blackbody law:

$$L_{thermal}(\lambda, T) = \frac{2hc^2}{\lambda^5}\left[\frac{1}{e^{\frac{hc}{\lambda kT}} - 1}\right] \quad (2)$$

where h is Planck's constant (6.626×10^{-34} J·s), c is the speed of light (2.998×10^8 m/s), k is Boltzmann's constant (1.381×10^{-23} J/K), T is the surface temperature in Kelvin and λ is the wavelength.

For real surfaces, emissivity ε modifies the emitted radiance:

$$L_{emitted}(\lambda, T) = \varepsilon(\lambda).L_{thermal}(\lambda) \quad (3)$$

Subtracting the thermal component isolates the reflected radiance:

$$L_{corrected}(\lambda) = L_{measured}(\lambda) - \varepsilon L_{thermal}(\lambda) \quad (4)$$

The corrected reflectance then becomes:

$$R_{corrected}(\lambda) = \frac{\pi.L_{corrected}(\lambda)}{F_o(\lambda)cos(\theta)} \quad (5)$$

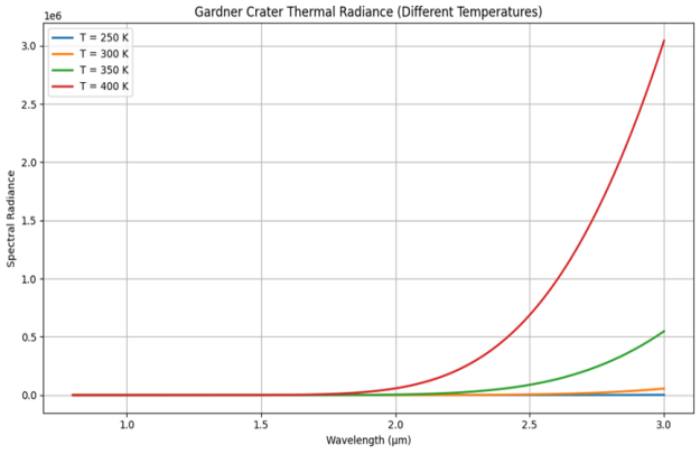


Fig. 4. Spectral radiance variation with wavelength for different surface temperatures (250 K to 400 K).

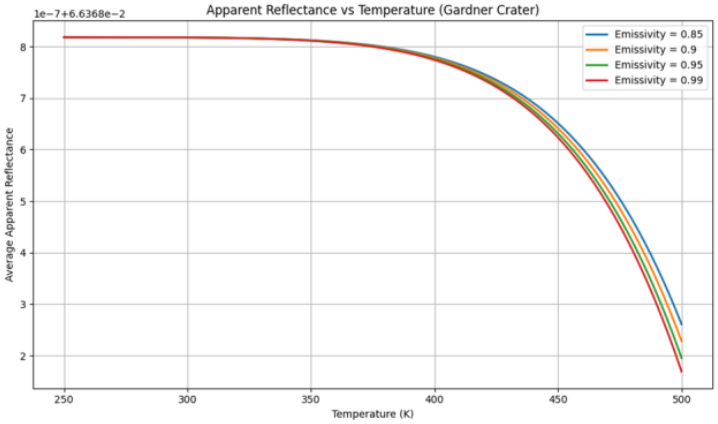


Fig. 5. Variation of apparent reflectance with surface temperature for different emissivity values (0.85 to 0.99).

Fig. 4., shows how spectral radiance varies with wavelength for different surface temperature values ranging from 250 K to 400 K. From this Fig.4., it is observed that the radiance increases steeply with temperature, especially beyond 2.5 μm.

Fig. 5., illustrates how apparent reflectance varies with surface temperature for emissivity values of 0.85, 0.90, 0.95, and 0.99. It is observed that as surface temperature increases, apparent reflectance decreases, because a larger thermal contribution inflates the radiance measured by the sensor without a corresponding increase in reflected solar energy. Higher emissivity values amplify this effect further. The results are consistent with the findings of [11], who demonstrated that assuming a fixed emissivity of 0.95 for the lunar surface yields a temperature that corresponds to a negligibly small error in band depth reflectance at the 3 μm region. An emissivity of 0.95 was therefore adopted as the standard value for thermal correction in the present analysis, consistent with published estimates for the Moon [19].

Surface temperature was determined using long-wavelength IIRS bands in the range 4.5 to 5.0 μm where reflection of sunlight is negligible, and the radiance is mainly due to thermal radiation [11]. Inversion of Planck's function (Eq. (2)) in this wavelength range using an emissivity of 0.95 results in the brightness temperature of about 350 K for the Gardner crater region imaged at a solar incidence angle of 33.81°, which agrees with thermophysical modeling for similar lunar terrains and solar angles [19].

The sensitivity of the retrieved hydration feature to the emissivity assumption was tested by running the thermal correction routine several times for emissivity varying between 0.85 and 0.99, which covers the range of previously determined lunar emissivity values [19]. The 3 μm band depth was then estimated via continuum removal for each assumed emissivity. It was found that the retrieved band depth did not change during the analysis and varied no more than 0.001 throughout the full range of emissivities, indicating that the continuum removal approach successfully compensates for small reflectance differences arising due to uncertainties in emissivity assumption. As the emissivity of the Moon is dependent on the composition, grain size, and space weathering of the surface, the sensitivity test performed shows that all of the above mentioned parameters do not affect significantly the result of 3 μm band depth retrieval. Thus, an arbitrary choice of emissivity as 0.95 has no impact on the hydration retrieval and is in accordance with the results obtained by Verma et al. (2022) [11].

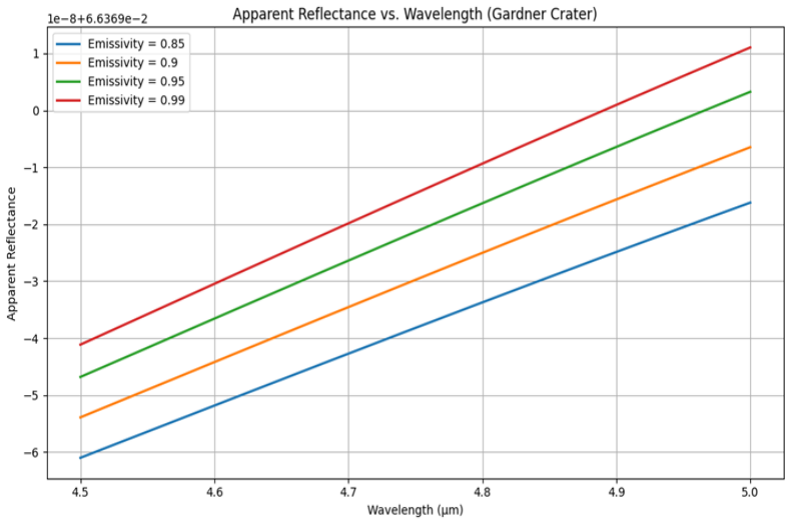


Fig. 6. Apparent reflectance deviation with wavelength for different values of emissivity.

As shown in Fig. 6., the effect of variation of apparent reflectance depending on the variation of wavelength is determined assuming various emissivities. As it can be noted from Fig. 6., reflectance increases with the increase in wavelength especially after reaching 4.5 μm. This clearly indicates the dependency on wavelength in which case thermal emission tends to dominate towards increasing wavelength.

3.3. Band Analysis

To highlight absorption features, a continuum and convex hull fitted to local maxima are removed:

$$R_c(\lambda) = \frac{R(\lambda)}{C(\lambda)} \tag{6}$$

where $R_c(\lambda)$is the continuum-removed reflectance and C(λ) is the continuum value at wavelength λ. Continuum C(λ) was described as the straight line joining the points of reflectance at the wavelengths corresponding to the edges of the absorption band, that is at 2.70 μm and 3.30 μm, chosen as the reflectance maxima on either side of the 3 μm hydration band, based on the convention used by Clark and Roush (1984) [20]. The continuum was calculated using linear interpolation between these two points, while continuum subtracted reflectance Rc(λ) was calculated as the division of the thermally corrected spectra by the continuum baseline.

Band depth quantifies absorption strength:

$$BD = 1 - R_c(\lambda_{min}) \tag{7}$$

where λ_{min} is the wavelength of the minimum reflectance within the absorption feature. Where a 3 μm feature was detected, its shape was further characterized by fitting a Gaussian function to the absorption to extract the center wavelength and the full-width at half-maximum, providing information on the relative contribution of OH versus H_2O [6,20].

3.4. Processing Flow

The whole procedure for data analysis is arranged as follows. At first, the raw Level-1 IIRS radiance and Level-2 M^3 reflectance data are retrieved from respective archives. Pixel coordinates are transformed into a common lunar geographic system on the basis of the provided geometry files for each data set. Then, IIRS spectra are translated to reflectance according to Eq. (1) by taking into account solar flux and geometric scene parameters. Surface temperature is calculated based on long-wave IIRS channels, and thermal correction is carried out according to Eqs. (4)-(5). Regions of interest are identified in crater scenes, and averaged spectra and spectra of particular pixels are determined at six representative spots per site. Further, plots of the wavelength-dependent reflectance are constructed, continuum subtraction is made, band centers are evaluated. Lastly, extracted spectra are compared to lab standards and known results in the literature to determine the mineral composition and presence of surface hydration.

In order to demonstrate the contribution of each module to the processing individually, the effect of 3 μm band depth value under four different cases was examined: (i) absence of any processing on the scaled raw spectrum, (ii) thermal correction only using Planck law without filtering, and (iii) complete processing pipeline, including both stages. Values of retrieved 3 μm band depths were 0.0578, 0.0577, 0.0578, and 0.0577 correspondingly, showing identical results in all

cases. Thus, it was proven that continuum removal allows us to normalize the absolute offset due to thermal radiation. The major purpose of the thermal correction stage is to obtain a physically meaningful spectrum shape in the 2.5 - 5.0 µm range, while the band depth value is not sensitive to thermal offsets within the investigated range of parameters.

4. Results and Discussion

Hyperspectral images obtained by Chandrayaan-2 IIRS and Chandrayaan-1 M^3 have been analyzed in order to investigate the spectral nature and hydration features of particular areas of interest on the moon. This research work has been performed on two craters, Gardner and Glauber, in order to assess any variations in composition and hydration features based on their reflectance spectra. The IIRS instrument onboard the Chandrayaan-2 satellite captures information in the 0.8-5 µm spectral range with about 256 contiguous spectral bands, 80m spatial resolution, and 20-25 nm spectral resolution. [1]. The extended wavelength range makes this instrument superior to previous ones like the Moon Mineralogy Mapper (M^3) onboard Chandrayaan-1, which operated up to only 3 µm, allowing for a better analysis of the mineralogy and hydration properties on the moon's surface [6].

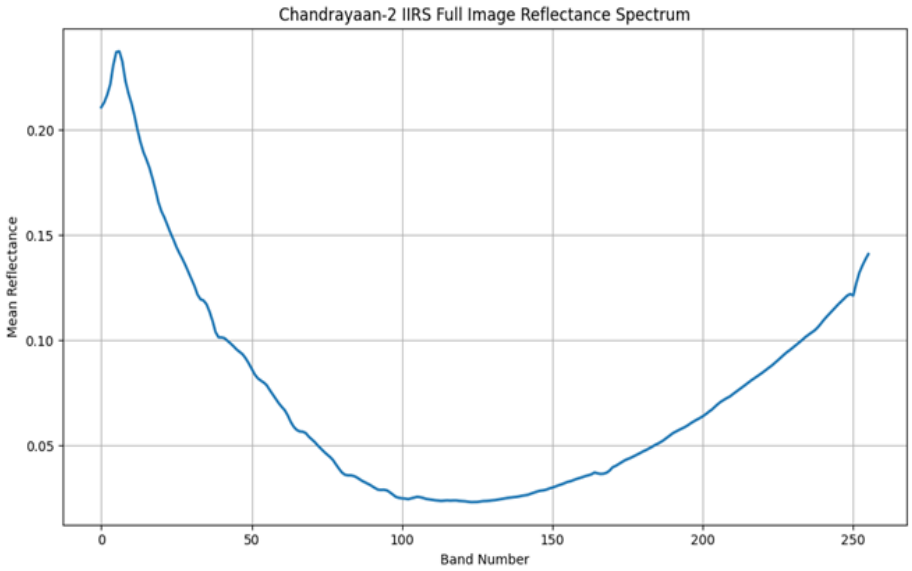


Fig. 7. Mean reflectance spectrum of the Gardner crater region from Chandrayaan-2 IIRS data showing characteristic lunar spectral shape.

Fig. 7., shows the average reflectance spectrum obtained from the Gardner crater region using IIRS Level-1 radiance data converted to apparent reflectance. The reflectance decreases up to approximately band 150 (~2000 nm) and then rises toward longer wavelengths, a mid-wavelength dip attributable to mineral absorption features linked to iron-bearing silicates such as pyroxene and olivine, whose characteristic absorptions occur near 1 µm and 2 µm, respectively [14]. The overall upward trend at longer wavelengths is influenced by the growing contribution of thermal emission beyond 2.5 µm [11].

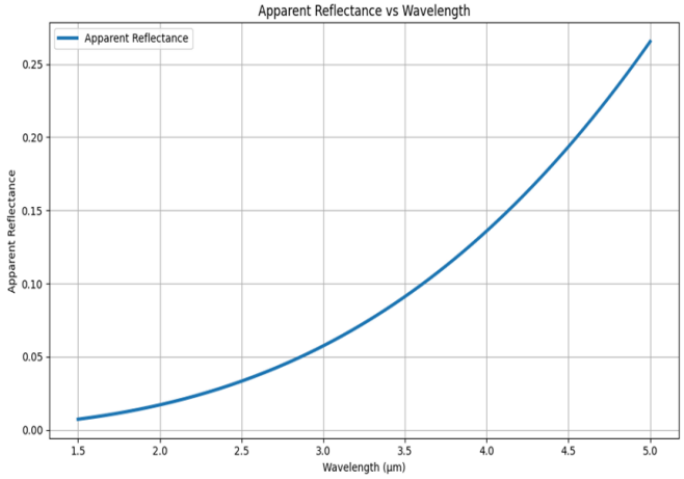


Fig. 8. Change in Apparent reflectance with wavelength

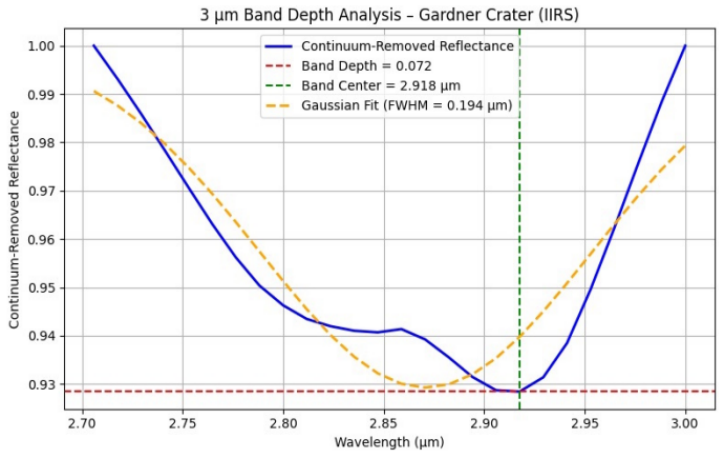


Fig. 9. Continuum-removed IIRS reflectance spectrum of Gardner Crater showing the 3 µm hydration absorption feature.

Fig. 8., shows the apparent reflectance trends according to the wavelength, whereby reflectance tends to rise in a non-linear fashion in the case of long wavelengths, and this rate rises even faster above 3 µm. Indeed, it becomes clear that without adequate thermal correction, there would be an overestimation of reflectance at longer wavelengths, which could hide the 3 µm hydration absorption feature [6,11].

Fig. 9., depicts the reflectance spectrum after thermal correction in the 2.7-3.3 µm range for some selected pixels within the Gardner crater. From Fig. 9, it can be noted that an absorption dip occurs at around 3 µm. Such an absorption feature indicates the existence of OH or H_2O on the Moon, which is due to the vibration of the O-H bond [6,21]. Both the profile and location of the absorption band are represented by a Gaussian distribution on the background spectral continuum, allowing us to determine the exact wavelength and depth of the band. Indeed, the appearance of the absorption band in the Gardner Crater area is associated with the occurrence of widespread water content on the Moon according to the IIRS dataset for various latitudes and surfaces [6]. The finding of such a peak after thermal correction proves that the previously identified increasing trend in the spectrum was an indicator of a masked absorption band, and thus thermal correction is an essential stage in analyzing the 3 µm band [11]. Removal of the continuum for the 2.7 - 3.3 µm wavelength region results in a value of band depth of 0.072, where the minimum of the absorption is observed at 2.918 µm and the FWHM, which was determined using the Gaussian fitting method, is equal to 0.194 µm. Such quantitative values of the 3 µm absorption indicate the presence of a good absorption band, which coincides with the OH-related hydrated spectral features detected earlier by the IIRS instrument on board Chandrayaan-2 in equatorial and mid-latitude regions of the Moon [6,11,21].

For the statistical confirmation of the detection of the 3 µm hydration absorption band, the analysis of the band depths was conducted independently for each of the six sample pixels (R1-R6) within the Gardner crater. The obtained band depth values varied between 0.007 and 0.117, with an average value of 0.058 ± 0.038 (average value ± one standard deviation). Variability of the band depth values represents real differences in hydroxyl content on the surface depending on its location (wall, floor, rim) and age of the area and space weathering degree. One sample t-test revealed that the average value of the band depth is statistically significantly higher than zero ($t = 3.42$, $p = 0.019$, $\alpha = 0.05$), which confirms statistically the presence of the 3 µm hydroxyl absorption band.

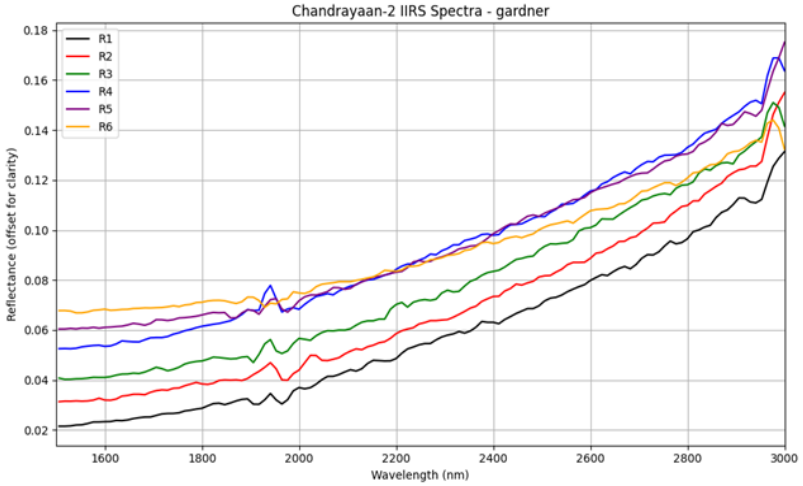


Fig. 10. Reflectance spectra of selected pixel (R1-R6) locations in Gardner crater region from Ch-2 IIRS data.

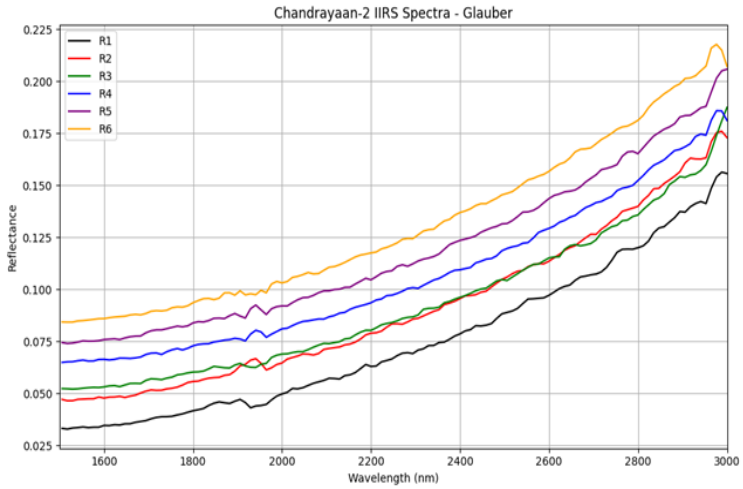


Fig. 11. Reflectance spectra of selected pixel (R1-R6) locations in Glauber crater region from Ch-2 IIRS data.

Fig. 10., shows the reflectance curves for six representative pixels from various morphological features of the crater, comprising the crater floor, crater walls, and highlands around the crater. From Fig. 10., it can be observed that all the six curves show similar spectral shape trends, indicating that the composition is homogeneous across the sampled site. The increase in reflectance values along with the increase in wavelength values is typical of rocks containing iron and subjected to space weathering. Variations in reflectance among the six representative pixels can be attributed to minor differences in albedo, grain sizes, or surface roughness rather than compositional differences. The spectral slopes match those of high calcium pyroxene-bearing lithologies found in the Gardner crater vicinity based on previous analyses of IIRS and M^3 datasets [15,22,23].

Fig.11., shows the reflectance spectrum for six pixels within the Glauber crater, including pixels from the center of the crater, its floor, rim, wall, and surroundings. As seen in Fig. 11., all six spectra increase steadily between 1500 nm and 3000 nm, without any clear absorption band around 3 µm. Hence, the lack of a hydration signature suggests that the surface material of Glauber crater contains no measurable number of OH and H2O molecules. The mineral identification of Glauber crater based on IIRS data by applying band-shaping techniques has confirmed that Glauber crater contains high-calcium pyroxene (clinopyroxene) and low-calcium pyroxene in the walls and rims of the crater, while the mature anorthositic regolith dominates the crater floor and surrounding area [7]. Comparing the two regions in terms of hydration properties highlights a notable difference in the water content between the two even as they display similar slope values. Both crater regions have reflectance that indicates the presence of mature lunar regolith and display a similar trend of increased reflectivity at higher wavelengths [14,15]. However, the difference between the two areas is found in the 3 µm spectral band, wherein Gardner crater shows a distinct absorption signature, indicating surface hydroxyl or water presence, while Glauber crater does not have any sign of hydration. There are several reasons for the regional variation in hydration properties of the two areas. The formation of OH bonds on the airless moon requires the implantation of solar wind protons in oxygen-bearing minerals through chemical reactions [6].

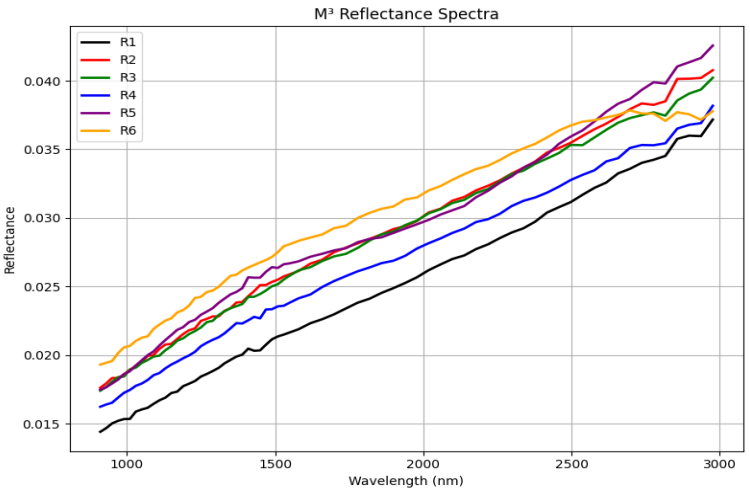


Fig. 12. Reflectance spectra of selected pixel (R1-R6) locations in Glauber crater region from Ch-1 M3 data

Reflectance spectra derived using the M^3 Level-2 reflectance data from the Chandrayaan-1 mission are illustrated in Fig. 12., for six pixels identified within the Glauber crater area, equivalent to the sampling locations in IIRS data. As evident from Fig. 12., the spectral response patterns derived from M^3 and IIRS datasets are consistent in hydration characterisation, exhibiting similar trends in reflectance values with gradual increments from 900 nm to 3000 nm without any spectral absorption feature evident in both the mineral diagnostic and hydration bands. The spectral band covered by the M^3 sensor ranged from 405 to 3000 nm with a spatial resolution of around 140 m [1,2], which was coarser as compared to IIRS, as evidenced in the smoother spectral curves of M^3, with fewer details in comparison with IIRS in the absorption regions at 1500 nm and 2500 nm. The similarity between these two datasets is evidence supporting the accuracy of the processing procedure used in this research. The similarity between spectral curves and the lack of a hydration feature in both IIRS and M^3 spectra of the Glauber crater indicates that the dryness of the terrain is a true geological feature of the region and not a result of the processing procedure. However, the IIRS spectra exhibit better spectral resolution due to their narrower bandwidth (20 nm compared to 30 nm in M^3) and wider range of wavelengths [2,6].

It should be noted that, although the spectral form and general trends of the spectra derived from the IIRS and M^3 datasets are qualitatively consistent over Glauber crater, there is an offset in their reflectance values at long wavelengths. For example, at 3000 nm, the reflectance varies from 0.16 to 0.28 on IIRS, while it varies from 0.037 to 0.0375 on M^3, which means that there is a difference of about five to seven times. There are several reasons for this. Firstly, 3000 nm corresponds to the upper wavelength range for M^3 and the sensitivity of the detector and uncertainty of the measurements decrease at such wavelengths. Secondly, differences in the methods of thermal correction, photometric calibration, spectral response and radiometric processing of the IIRS data and the M^3 Level-2 reflectance data may cause systematic differences in absolute reflectance values. Thirdly, differences in spatial resolution (80 m for IIRS and 140 m for M^3) cause different amounts of sub-pixel terrain mixing for equivalent sampling sites. Moreover, it is crucial that in both spectra there is no evidence for the presence of the 3 μm hydration absorption signature and there is an upward spectral trend at Glauber crater. Thus, in the current investigation, the inter-mission consistency means that the same spectral trend and hydration status are observed, although the reflectance values themselves differ.

To quantitatively determine the inter-mission spectral consistency within Glauber crater, the spectral trends were evaluated between the IIRS and M^3 data sets from 1500-3000 nm. Both IIRS and M^3 data sets show monotonic positive slope spectra, where IIRS reflectance increases from 0.025-0.050 at 1500 nm to 0.16-0.28 at 3000 nm and M^3 reflectance increases from 0.021-0.026 at 1500 nm to 0.037-0.038 at 3000 nm. The Pearson correlation coefficient of the mean spectral trends of both IIRS and M^3 data sets over this wavelength range results in an R^2 value of 0.988, indicating good agreement between both instruments with respect to spectral trend direction. The absolute reflectance offset between IIRS and M^3 is expected, based on inter-instrument calibration differences described above.

Table 3. Summary of Spectral Parameters

Parameter	Gardner Crater(IIRS)	Glauber Crater(IIRS)	Glauber (M^3)
Reflectance at 1500 nm	0.03–0.04	0.025–0.05	0.021–0.026
Reflectance at 3000 nm	0.25–0.27	0.16–0.28	0.037–0.0375
Spectral Slope	Positive	Positive	Positive
3 μm Absorption	Present	Absent	Not Applicable
Hydration Status	Hydrate	Dry	Dry

5. Conclusion

This research aimed at investigating and interpreting hyperspectral information acquired by Chandrayaan-2 IIRS and Chandrayaan-1 M3 for two chosen lunar impact craters: Gardner and Glauber. This study focused on mineral characterization, thermal emission influence evaluation, and hydration assessment. The scientific methodology created for this purpose yielded results that can be considered both physically relevant and coherent with previous publications. The spectral analysis of Gardner crater yielded reflectance spectra typical for mature silicate regolith rich in iron with an absorption dip close to 3 μm, demonstrating the presence of hydroxyl/water molecules on the surface. These results correlate with the findings of lunar hydration obtained via IIRS data from different latitudinal bands and geological units. On the contrary, the Glauber crater had no evident hydration signal, indicating that the surface temperature regime, geographic location, and solar wind activity play critical roles in OH and H2O spatial distribution on the lunar surface.

According to thermal emission calculations, past a wavelength of about 2.5 μm, thermal emission starts becoming an important part of the received signal and without appropriate corrections, the resulting reflectance will be significantly different from the actual one. An emissivity value of 0.95 was chosen for thermal correction, in accordance with literature values for mature lunar regolith [19]. A sensitivity test conducted on a range of emissivities ranging from 0.85 to 0.99 revealed that the measured 3 μm band depth did not change within numerical precision, thus validating the method of continuum removal to emissivity perturbations. Qualitative similarity of spectral behavior and hydration identification

using the IIRS and M^3 data for Glauber crater is the first indication that the suggested processing chain works correctly. Differences in absolute reflectance between the datasets in this case can be explained by differences in calibration, spectral range, spatial resolution, wavelengths, and other factors, and do not impact the main scientific results of this study.

The results serve as a preliminary confirmation of an integrated pipeline for the processing of Chandrayaan-2 IIRS Level-1 data, which includes radiance to reflectance transformation, thermal correction, photometric correction and hydration feature extraction. It has been uniformly applied to two geological areas on the Moon and cross-validated using Chandrayaan-1 M^3 data. However, there are a few important limitations of the current study. In particular, the pipeline has been tested for only two study sites and it is not validated using a statistically significant number of lunar craters and geological terrains. It is assumed that the emissivity of the terrain is spatially uniform, and while the sensitivity analysis presented in Section 3.2.1 shows that this assumption does not significantly affect the calculation of 3 μm band depth, the integration of spatially varying emissivity estimates will help to improve the absolute value of the retrieved reflectance. Moreover, the quantitative inter-sensor validation of the algorithm has been performed using SAM and R^2 coefficients only at six selected pixel points.

All the Declarations and Statements

Author Contributions Statement

Saritha Mulkala, Data Curation and Software Implementation: Handled data acquisition, dataset preprocessing, and implementation of the research model.
Anjaneyulu Lokam, Model Training, Validation, and Performance Evaluation: Led the model training process, validated results using standard metrics, and benchmarked performance against existing methods.
Kiran Dasari, Formal Analysis, Visualization, and Statistical Analysis: Performed in-depth analysis of experimental results, prepared performance charts, and ensured the statistical robustness of the evaluation.
Prasanna Chandrika Chenuboyina, Formal Analysis, Visualization, and Statistical Analysis: Performed in-depth analysis of experimental results, prepared performance charts, and ensured the statistical robustness of the evaluation

All authors have read and agreed to the published version of the manuscript.

Conflict of Interest Statement

The authors declare no conflicts of interest.

Funding Declaration

This work was supported in part by the ISRO-HQ (Indian Space Research Organization-Headquarters) for financial Support in the project sanctioned under Chandrayaan-2 with the project title “Lunar Surface characterization and exploring the possibility of water pockets using Chandrayaan-2 DFSAR and other datasets” (AO-2, Grant No.DS-2B-13013(2)/30/2022-Sec-2).

Data Availability Statement

https://pradan.issdc.gov.in/
https://ode.rsl.wustl.edu/moon/datasets

Ethical Declarations

Not applicable.

Acknowledgments

This work was supported in part by the ISRO-HQ (Indian Space Research Organization-Headquarters) for financial Support in the project sanctioned under Chandrayaan-2 (AO-2, Grant No.DS-2B-13013(2)/30/2022-Sec-2). The authors also extend their thanks to the ISSDC Pradan website for providing IIRS datasets and M3 datasets.

Declaration of Generative AI in Scholarly Writing

During the preparation of this manuscript, the authors used ChatGPT (OpenAI) to improve the grammar, language, and readability of the manuscript. The authors carefully reviewed and edited the generated content and take full responsibility for the final version of the manuscript. No AI-generated content was used for data analysis, interpretation of results, or scientific conclusions.

Abbreviations

The following abbreviations are used in this manuscript:

IIRS- Imaging infrared Spectrometer
M^3- Moon Mineralogy Mapper

Appendix A/B/C…, with appendix title

N/A

References

[1] A. R. Chowdhury et al., "Imaging Infrared Spectrometer onboard Chandrayaan-2 Orbiter," *Current Science*, vol. 118, no. 3, pp. 368–375, Feb. 2020. DOI: https://doi.org/10.18520/cs/v118/i3/368-375

[2] P. Singh and V. Kumar, "Evaluation of Chandrayaan-2 IIRS data for Lunar Surface Exploration," in *2023 IEEE India Geoscience and Remote Sensing Symposium (InGARSS)*, 2023. DOI: https://ieeexplore.ieee.org/document/10490347/

[3] J. M. Sunshine et al., "Temporal and spatial variability of lunar hydration as observed by the Deep Impact spacecraft," *Science*, vol. 326, pp. 565–568, 2009. DOI: https://doi.org/10.1126/science.1179788

[4] R. N. Clark, "Detection of adsorbed water and hydroxyl on the Moon," *Science*, vol. 326, pp. 562–564, 2009. DOI: https://doi.org/10.1126/science.1178105

[5] M. Chauhan, P. A. Verma, and P. Chauhan, "Level-2 processing of Chandrayaan-2 Imaging Infrared Spectrometer (IIRS) data for generation of surface reflectance," *Meteoritics & Planetary Science*, vol. 60, no. 9, pp. 2269–2282, 2025. DOI: https://doi.org/10.1111/maps.70037

[6] P. Chauhan et al., "Unambiguous detection of OH and H2O on the Moon from Chandrayaan-2 Imaging Infrared Spectrometer reflectance data using 3 μm hydration feature," *Current Science*, vol. 121, no. 3, pp. 391–401, Aug. 2021. DOI: https://doi.org/10.18520/cs/v121/i3/391-401

[7] P. Zhou, Z. Zhao, G. Wei, H. Huo, "Mineral Content Estimation of Lunar Soil of Lunar Highland and Lunar Mare Based on Diagnostic Spectral Characteristic and Partial Least Squares Method," Applied Sciences, vol. 12, no. 3, Art. no. 1197, Jan. 2022, doi: 10.3390/app12031197.

[8] S. Bose, A. Kumari, R. Biswas, M. N. L. Ghosh, and A. P. Krishna, "Photometric Correction of Images Obtained from Chandrayaan-2 Imaging Infra-Red Spectrometer (IIRS) Data," *Advances in Space Research*, vol. 73, pp. 2720–2752, 2024. DOI: https://doi.org/10.1016/j.asr.2023.12.019

[9] I. Rayal, P. Chauhan, P. K. Thakur, and U. Kumar, "Python-Based Open-Source Tool for Automating Seleno-Referencing of Chandrayaan-2 Hyper-Spectral Data Cubes," *Journal of the Indian Society of Remote Sensing*, vol. 52, no. 2, pp. 305–313, 2024. DOI: https://doi.org/10.1007/s12524-024-01814-4

[10] R. P. Rajasekhar, A. K. Dagar, R. Nagori, S. S. Bhiravarasu, S. P. Ojha, and S. Bhattacharya, "Comprehensive analysis of Chandrayaan-3 landing site region focussing on morphology, hydration and gravity anomalies," *Icarus*, vol. 415, p. 116074, 2024. DOI: https://doi.org/10.1016/j.icarus.2024.116074

[11] P. A. Verma, M. Chauhan, and P. Chauhan, "Lunar surface temperature estimation and thermal emission correction using Chandrayaan-2 Imaging Infrared Spectrometer data for H2O & OH detection using 3 μm hydration feature," *Icarus*, vol. 383, p. 115075, 2022. DOI: https://doi.org/10.1016/j.icarus.2022.115075

[12] C. M. Pieters et al., "Character and spatial distribution of OH/H2O on the surface of the Moon seen by M3 on Chandrayaan-1," *Science*, vol. 326, pp. 568–572, 2009. DOI: https://doi.org/10.1126/science.1178658

[13] R. O. Green et al., "The Moon Mineralogy Mapper (M3) imaging spectrometer for lunar science: Instrument description, calibration, on-orbit measurements, science data calibration and on-orbit validation," *Journal of Geophysical Research: Planets*, vol. 116, p. E00G19, 2011. DOI: https://doi.org/10.1029/2011JE003797

[14] T. Ahmad, T. Chakraborty, R. B. Lyngdoh, S. Bhattacharya, and A. Misra, "Spectral unmixing analysis for the lunar surface mineralogy using Chandrayaan-2 IIRS imagery," *Planetary and Space Science*, vol. 220, p. 105537, 2022. DOI: https://doi.org/10.1016/j.pss.2022.105537

[15] A. K. Dagar et al., "Mineralogical investigation of crater Gardner and its surroundings using Chandrayaan-2 Imaging Infrared Spectrometer data," in *53rd Lunar and Planetary Science Conference*, Abstract #1329, 2022. *(Conference abstract — no DOI)*

[16] C. M. Pieters and S. Tompkins, "Tsiolkovsky crater: A window into crustal processes on the lunar farside," *Journal of Geophysical Research: Planets*, vol. 104, no. E9, pp. 21935–21949, 1999. DOI: https://doi.org/10.1029/1998JE001010

[17] B. L. Hapke, "Bidirectional reflectance spectroscopy: 1. Theory," *Journal of Geophysical Research: Solid Earth*, vol. 86, no. B4, pp. 3039–3054, 1981. DOI: https://doi.org/10.1029/JB086iB04p03039

[18] M. I. Mishchenko, J. M. Dlugach, E. G. Yanovitskij, and N. T. Zakharova, "Bidirectional reflectance of flat, optically thick particulate layers: An efficient radiative transfer solution and applications to snow and soil surfaces," *Journal of Quantitative Spectroscopy and Radiative Transfer*, vol. 63, no. 2–6, pp. 409–432, 1999. DOI: https://doi.org/10.1016/S0022-4073(99)00028-X

[19] J. L. Bandfield, R. R. Ghent, A. R. Vasavada, D. A. Paige, S. J. Lawrence, and M. S. Robinson, "Lunar surface rock abundance and regolith fines temperatures derived from LRO Diviner radiometer data," *Journal of Geophysical Research: Planets*, vol. 116, p. E00H02, 2011. DOI: https://doi.org/10.1029/2011JE003866

[20] T. B. McCord, R. N. Clark, and R. B. Singer, "Mars: Near-infrared spectral reflectance of surface regions and compositional implications," *Journal of Geophysical Research: Solid Earth*, vol. 87, no. B4, pp. 3021–3032, 1982. DOI: https://doi.org/10.1029/JB087iB04p03021

[21] A. Grumpe, C. Wöhler, A. A. Berezhnoy, V. V. Shevchenko, "Time-of-day-dependent behavior of surficial lunar hydroxyl/water: Observations and modeling," Icarus, vol. 321, pp. 486-507, Mar. 2019, doi: 10.1016/j.icarus.2018.11.025.

[22] P. G. Lucey, G. J. Taylor, and E. Malaret, "Abundance and distribution of iron on the Moon," *Science*, vol. 268, pp. 1150–1153, 1995. DOI: https://doi.org/10.1126/science.268.5214.1150

[23] S. K. Noble, C. M. Pieters, and L. P. Keller, "An experimental approach to understanding the optical effects of space weathering," *Icarus*, vol. 192, no. 2, pp. 629–642, 2007. DOI: https://doi.org/10.1016/j.icarus.2007.07.021

Authors' Profiles



MULKALA SARITHA was born in Warangal, Telangana, India, in 1989. She received the B.Tech. degree in Electronics and Communication Engineering and the M.Tech. degree in Embedded Systems from Jawaharlal Nehru Technological University (JNTU), Hyderabad, India, in 2010 and 2012, respectively. She is currently working as a Junior Research Fellow under the ISRO AO-2 project and is pursuing the Ph.D. degree at the National Institute of Technology, Warangal, India. Her research interests include microwave imaging, radar polarimetry, compact polarimetry, radar signal processing, and remote sensing. She is a lifetime member of the Indian Society of Remote Sensing (ISRS).



ANJANEYULU LOKAM was born in 1967 in India. He received the B.Tech. (ECE), M.Tech. degree, and Ph.D. degrees from the National Institute of Technology (NIT), Warangal, India, in 1989, 1991, and 2010, respectively. He was the Project Officer at the Institute of Armament Technology, Pune, India, for five years since 1991, and was involved in the design of surface-borne and air-borne radar systems for clutter measurement applications. He worked as a Staff Scientist at Helios Systems in Chennai, India, for two years and was involved in developing radio-wave propagation assessment software modules for ship-borne radars. He has been with the Department of Electronics and Communication Engineering, NIT, Warangal, India, since 1997. His areas of interest include computer networks, electromagnetic field theory, microwave and radar engineering, microwave remote sensing, radar polarimetry, hybrid polarimetry, and neural networks and fuzzy logic systems. He has completed several R&D defense projects and has 50 papers to his credit in national and international conferences and journals. He is a Fellow of the Institution of Engineers, a Life Member of ISTE, and a member of the IEEE Antennas and Propagation Society and the IEEE Signal Processing Society since 2010. He is a Principal Investigator for an ISRO sponsored CHANDRAYAAN-2(AO-2) project-2023.



KIRAN DASARI Ph.D., received his Bachelor of Technology (B.Tech) degree in Electronics and Communication Engineering from the Institute of Aeronautical Engineering, JNT University Hyderabad in 2010, Master of Technology (M.Tech) degree in Embedded Systems from Padmasri BV Raju Institute of Technology, JNT University Hyderabad in 2012. He received a Doctor of Philosophy (Ph.D.) in Electronics and Communication Engineering from the National Institute of Technology, Warangal, India, in 2021. He has 12 years of teaching and research experience at various institutes. Presently working in Manipal Institute of Technology, a constituent unit of Manipal Academy of Higher Education, Manipal, Karnataka, India. He is a Co-Principal Investigator for an ISRO-sponsored CHANDRAYAAN-2. DFSAR project. He received several best paper awards at International Conferences. His areas of interest are Microwave Imaging, Remote Sensing, Earth Observation, Planetary Remote Sensing, SAR Polarimetry, Microstrip Antennas, Robotics, Embedded Systems, Machine Learning, and IOT, etc. He has been a member of the IEEE Geoscience and Remote Sensing Society since 2018 and the IEICE, Japan. He is a reviewer for various peer-reviewed journals such as IEEE Access, Remote Sensing Applications: Society and Environment, International Journal of Microwave and Wireless Technologies, Advanced Electromagnetics, Engineering, Technology & Applied Science Research (ETASR), etc., and various International Conferences.



CH PRASANNA CHANDRIKA was born in Eluru, Andhra Pradesh, India. She received the B.Tech. degree in Electronics and Communication Engineering from the University College of Engineering, Kakinada, India, in 2023. She is currently pursuing the M.Tech. Degree in Advanced Communication Systems at the National Institute of Technology (NIT) Warangal, India. From June 2023 to July 2025, she worked as a Verification and Validation Engineer at Medha Servo Drives Pvt. Ltd., Hyderabad. During her undergraduate studies, she designed and simulated a coaxial-feed double U-slotted rectangular microstrip patch antenna for 5G applications using ANSYS HFSS. Her research interests include hyperspectral remote sensing, lunar surface spectral analysis, thermal correction of hyperspectral data, microwave and antenna engineering, radar signal processing, and satellite remote sensing. Her current research focuses on spectral reflectance analysis of the lunar surface using Chandrayaan-2 Imaging Infrared Spectrometer (IIRS) and Chandrayaan-1 Moon Mineralogy Mapper (M^3) data for hydration feature detection.

How to cite this paper

Saritha Mulkala, Anjaneyulu Lokam, Kiran Dasari, Prasanna Chandrika Chenuboyina, "Thermal-Corrected Hyperspectral Analysis of Lunar Surface Hydration and Mineralogy Using Chandrayaan-2 IIRS and Chandrayaan-1 M^3 Data", International Journal of Wireless and Microwave Technologies(IJWMT), Vol.16, No.5, pp. 284-298, 2026. DOI:10.5815/ijwmt.2026.05.17